CrossMark

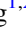# Is GRB 110715A the Progenitor of FRB 171209?

Xiang-Gao Wang[1,2] , Long Li[1,2,3], Yuan-Pei Yang[4] , Jia-Wei Luo[5], Bing Zhang[5] , Da-Bin Lin[1,2] , En-Wei Liang[1,2] , and Song-Mei Qin[6]

[1] Guangxi Key Laboratory for Relativistic Astrophysics, School of Physical Science and Technology, Guangxi University, Nanning 530004, People's Republic of China; wangxg@gxu.edu.cn
[2] GXU-NAOC Center for Astrophysics and Space Sciences, Nanning 530004, People's Republic of China
[3] School of Astronomy and Space Science, Nanjing University, Nanjing 210093, People's Republic of China
[4] South-Western Institute for Astronomy Research, Yunnan University, Kunming 650500, People's Republic of China; ypyang@ynu.edu.cn
[5] Department of Physics and Astronomy, University of Nevada Las Vegas, NV 89154, USA; zhang@physics.unlv.edu
[6] Mathematics and Physics Section, Guangxi University of Chinese Medicine, Nanning 53001, People's Republic of China

Abstract

The physical origin of fast radio bursts (FRBs) is unknown. Young magnetars born from gamma-ray bursts (GRBs) have been suggested as a possible central engine of FRBs. We test such a hypothesis by systematically searching for GRB–FRB spatial associations from 110 FRBs and 1440 GRBs. We find that one FRB event discovered by the Parkes telescope, FRB 171209, is spatially coincident with a historical long-duration GRB 110715A at $z = 0.82$. The afterglow of GRB 110715A is consistent with being powered by a millisecond magnetar. The extragalactic dispersion measure of FRB 171209 is in excess of that contributed by the intergalactic medium, which can be interpreted as being contributed by a young supernova remnant associated with the GRB. Overall, the significance of the association is $(2.28–2.55)\sigma$. If the association is indeed physical, our result suggests that the magnetars associated with long GRBs can be the progenitors of at least some FRBs.

Unified Astronomy Thesaurus concepts: Radio transient sources (2008); Gamma-ray sources (633); Magnetars (992)

1. Introduction

Fast radio bursts (FRBs) are mysterious radio transients with millisecond durations, extremely high brightness temperatures, and large dispersion measures (DMs; e.g., Lorimer et al. 2007; Thornton et al. 2013; Cordes & Chatterjee 2019; Petroff et al. 2019). Their DMs are in excess of the Galactic contribution and the precise localizations of the host galaxies of a few FRBs suggest that they are extragalactic (e.g., Lorimer et al. 2007; Thornton et al. 2013; Chatterjee et al. 2017; Bannister et al. 2019; Prochaska et al. 2019; Ravi et al. 2019; Marcote et al. 2020). A persistent radio emission with luminosity of $L \sim 10^{39}$ erg s^{-1} at a few GHz was discovered to be spatially coincident with FRB 121102, which showed a non-thermal spectrum that deviates from a single power-law spectrum from 1 to 26 GHz (Chatterjee et al. 2017). One possibility is that such a persistent radio emission source originates from a shocked nebula associated with a young magnetar born in a supernova (SN) or a gamma-ray burst (GRB; Murase et al. 2016; Metzger et al. 2017). On the other hand, there is no confirmed multiwavelength transient being associated with any FRB (e.g., Petroff et al. 2015; Callister et al. 2016; Gao & Zhang 2017; Zhang & Zhang 2017; MAGIC Collaboration et al. 2018; Tingay & Yang 2019). There might be three main reasons for this. 1. The fluxes of the multiwavelength counterparts of FRBs are low, e.g., for typical parameters, the FRB afterglows are very faint (Yi et al. 2014). 2. The duration of the multiwavelength transient may be shorter than the time resolution of a detector, e.g., the prompt high-energy emission associated with the FRB itself (Yang et al. 2019b). 3.

the time delay between the multiwavelength transient and the FRB is longer than the observation time, e.g., FRBs emitted from a young magnetar born from a catastrophic event (such as a GRB or a SN) may have a long delay with respect to the event itself (Murase et al. 2016; Metzger et al. 2017).

Without confirmed multiwavelength transients associated with FRBs, the physical origin of FRBs remain unknown. The current FRB models can be divided into two categories[7]: catastrophic models (e.g., Kashiyama et al. 2013; Totani 2013; Falcke & Rezzolla 2014; Zhang 2014, 2016; Liu et al. 2016; Wang et al. 2016) and non-catastrophic models (e.g., Dai et al. 2016; Murase et al. 2016; Metzger et al. 2017; Zhang 2017, 2020; Margalit & Metzger 2018; Ioka & Zhang 2020; Wang et al. 2020). The former suggest that an FRB is directly associated with a catastrophic event, and the time delay between the FRB and the catastrophic event is short. The latter usually involves a compact star, e.g., a neutron star or a black hole, that was born in a catastrophic event as the progenitor of an FRB. As the compact star can exist for a much longer time, the time delay between the FRB and the catastrophic event is allowed to be relatively long.

GRBs are the most luminous catastrophic events, and are produced by the core collapse of massive stars or binary compact star mergers (Mészáros 2006; Zhang 2018b). Although GRBs are much rarer than FRBs, the following reasons have been raised to suggest that a fraction of FRBs could be associated with GRBs. 1. An FRB might occur when a supermassive magnetar born in a GRB collapses into a black hole, the so-called "blitzar" scenario (Falcke & Rezzolla 2014; Zhang 2014). 2. An FRB might be related to the merger of a binary neutron star that produces a short GRB (Totani 2013;

---

[7] A complete list of FRB progenitor models can be found in Platts et al. (2019).

Wang et al. 2016). 3. A GRB as the source of astrophysical stream could interact with the magnetosphere of a neutron star to produce an FRB (Zhang 2017). 4. A GRB could produce a young magnetar that emits FRBs at a much later epoch (e.g., Metzger et al. 2017; Margalit et al. 2019; Wang et al. 2020). In the first three scenarios, an FRB could occur from milliseconds before to a few thousand seconds after the GRB. The fourth scenario allows a much longer delay of FRBs with respect to the GRB. Related to this, recently Eftekhari et al. (2019) discovered a radio source coincident with the superluminous SN (SLSN) PTF10hgi, similar to the persistent radio emission of FRB 121102 (Chatterjee et al. 2017), about 7.5 yr post-explosion, which might be emitted by the magnetar born in the SLSN. However, to date no FRB has been detected from the source.

In general, the searches for GRB–FRB associations have so far yielded no confirmed results (e.g., Bannister et al. 2012; Palaniswamy et al. 2014; DeLaunay et al. 2016; Scholz et al. 2016; Yamasaki et al. 2016; Xi et al. 2017; Zhang & Zhang 2017; Cunningham et al. 2019; Guidorzi et al. 2019; Yang et al. 2019a; Tavani et al. 2020). In particular, Men et al. (2019) recently performed dedicated observations of the remnants of six GRBs with evidence of having a magnetar central engine, but these observations did not lead to detection of any FRB from these remnants during a total of ~20 hr of observations.

In this work, we adopt a different approach to test the hypothesis that GRBs can be the progenitor of FRBs. We systematically search for GRB–FRB association events based on the precise localization of GRB afterglows, allowing a few years of time delay between a GRB and an FRB. Observationally, GRBs are typically localized by the Neil Gehrels Swift Observatory, i.e., the burst is detected by Swift/Burst Alert Telescope (BAT) and quickly localized by Swift/X-ray Telescope (XRT) with a several-arcsecond error bar, and later further localized by Swift/Ultraviolet/Optical Telescope (UVOT) or ground-based telescopes to subarcsecond precision. Based on the archival Swift/XRT and optical observational data, we search for possible GRB–FRB spatial association candidates. We detect one possible association between FRB 171209 (Osłowski et al. 2019) and GRB 110715A at $z = 0.82$ (Sánchez-Ramírez et al. 2017). This Letter is organized as follows. In Section 2, we present the search method and result. The GRB 110715A–FRB 171209 association is discussed in Section 3 in detail. The results are summarized with discussion in Section 4. Throughout the Letter, we adopt a concordance cosmology with parameters $H_0 = 71 \, \mathrm{km \, s^{-1} \, Mpc^{-1}}$, $\Omega_M = 0.30$, $\Omega_\Lambda = 0.70$, and temporal and spectral slopes of GRB afterglow emission are defined as $F \propto t^{-\alpha}\nu^{-\beta}$. Moreover, the convention $Q = 10^n Q_n$ is adopted in cgs units.

2. Search for GRBs Associated with FRBs in Archival Swift/XRT and Optical Observational Data

Since the discovery of the first FRB (Lorimer et al. 2007), 110 FRBs have been reported in the literature as of 2020 February[8] (e.g., Petroff et al. 2015; Casentini et al. 2020; CHIME/FRB Collaboration et al. 2019). Meanwhile, to date there are 1440 GRBs that have afterglow detections, including 845 GRBs with optical detections and 595 with Swift/XRT[9]
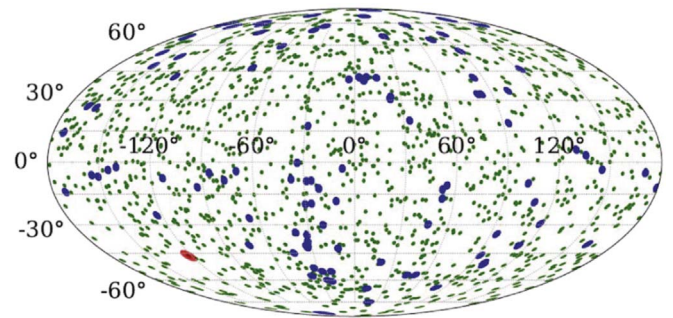

Figure 1. Sky celestial coordinate distributions of 110 FRBs and 1440 GRBs in our sample. The FRBs and GRBs are marked with blue and green circles, respectively. The positions of GRB 110715A and FRB 171209 are highlighted with a red circle.
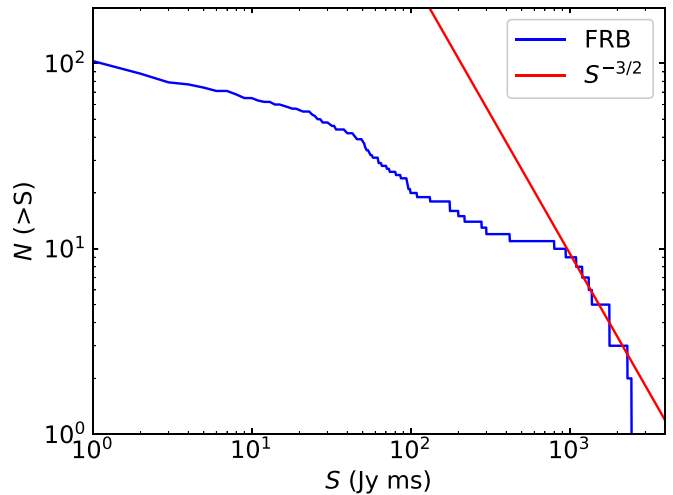

Figure 2. The $\log N - \log S$ distribution of the FRBs in our sample.

detections only. Among them, the numbers of long- and short-duration GRBs are 1320 and 120, respectively. Figure 1 shows the sky distribution of our samples (110 FRBs and 1440 GRBs) in celestial coordinates. The GRBs in our sample show a large-scale isotropic distribution, which is well known from the Burst and Transient Source Experiment (BATSE) observations (Briggs et al. 1996). Although the sample size of FRBs is smaller than that of GRBs, the FRBs in our sample also show an isotropic distribution, consistent with their cosmological origin. As shown in Figure 2, the distributions of the FRB fluence $(\log N - \log S)$[10] show a tendency with $N(>S) \propto S^{-3/2}$ at high S values. The deviation from the 3/2 power law is evident at low S values, which may be related to the spatial inhomogeneity effect and likely also observational biases and instrumental effects.

We perform a systematic search for GRBs that satisfy the following three criteria: (1) the GRB position is consistent with that of an FRB; (2) the GRB occurred earlier than the FRB if a position coincidence is discovered; (3) the redshift of the GRB is lower than the maximum FRB redshift derived from its DM.

We found only one GRB that is located at the position of an FRB, i.e., the GRB 110715A–FRB 171209 spatial association. GRB 110715A was triggered by the Swift/BAT on 2011 July 15 (UT dates are adopted) at 13: 13: 50 (T_0), with $T_{90} = 13$ s (Sonbas et al. 2011; Ukwatta et al. 2011). It was also detected
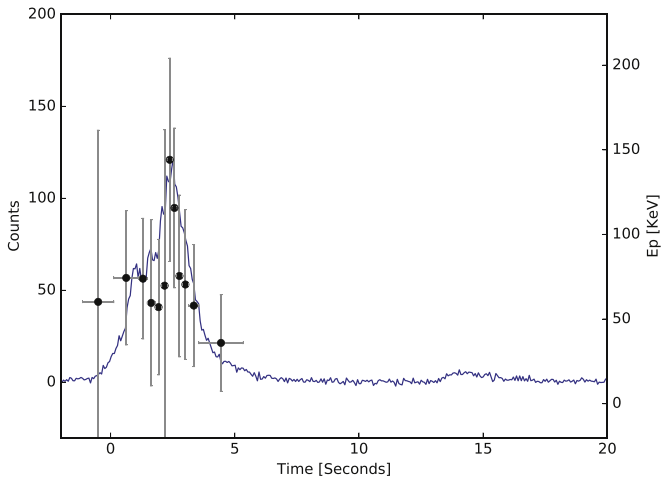

Figure 3. BAT light curve (blue line) and its E_p black circle evolution of GRB 110715A. The isotropic γ-ray energy is $E_{\gamma,\text{iso}} = (1.06 \pm 0.10) \times 10^{53}$ erg in the 1–10^4 keV band.

by the Konus-wind (Golenetskii et al. 2011). The Swift/XRT and Swift/UVOT began observing its X-ray and optical afterglows at 90.9 and 99 s after the BAT trigger, respectively (Evans & Sonbas 2011; Kuin & Sonbas 2011). It was also followed up by the Gamma-Ray Burst Optical/Near-Infrared Detector (GROND; Updike et al. 2011) and American Association of Variable Star Observers (AAVSO; Nelson 2011) ground-based optical telescopes; the Atacama Pathfinder Experiment (APEX; de Ugarte Postigo et al. 2011) and Atacama Large Millimeter/submillimeter Array (ALMA; Sánchez-Ramírez et al. 2017) submm telescopes; and the Australia Telescope Compact Array (ATCA; Hancock et al. 2011) radio telescope. The position of GRB 110715A, defined by its optical afterglow, is (R.A.$_{\text{J2000.0}}$, decl.$_{\text{J2000.0}}$) = ($15^{\text{h}}50^{\text{m}}44\overset{\text{s}}{.}09$, $-46°14'06''.53$), with an estimated uncertainty of $0''.56$ (radius, 90% confidence; Kuin & Sonbas 2011). The redshift of GRB 110715A was measured to be $z = 0.82$ (Piranomonte et al. 2011).

On the other hand, FRB 171209 (Osłowski et al. 2019) was detected 2338 days (~6.4 yr) after the GRB 110715A trigger. It was the first FRB detected as part of the commensal search during Parkes Pulsar Timing Array (PPTA) observations, with a position (R.A.$_{\text{J2000.0}}$, decl.$_{\text{J2000.0}}$) = ($15^{\text{h}}50^{\text{m}}25^{\text{s}}$, $-46°10'20''$), with an uncertainty of $7'.5$ (radius, 2.355σ confidence). The DM value is 1457.4 ± 0.03 cm^{-3} pc and the DM value contribution from the Milky Way is $\text{DM}_{\text{gal}} = 235$ cm^{-3} pc (Osłowski et al. 2019). Using a simple DM-z relation $\text{DM}_{\text{IGM}} \sim 855$ pc cm^{-3}z (Zhang 2018a), one can estimate the maximum redshift of FRB 171209, which is ~$(\text{DM}-\text{DM}_{\text{gal}})/855$ pc cm$^{-3} = 1.43$. Due to the existence of large-scale structures, the uncertainty of the DM contributed by the intergalactic medium (IGM) is about $\sigma_{\text{IGM}} \sim 300$ pc cm^{-3}. Thus the maximum redshift is constrained in the range of $z < (1.08\text{–}1.78)$. This is larger than the redshift of GRB 110715A.

To calculate of chance possibility for the putative GRB 110715A–FRB 171209 association, we assume that the spatial distribution of GRBs is isotropic and the number of GRBs within a specific sky area and time interval satisfies the Poisson distribution. The chance probability of having at least one GRB in the error circle of one FRB can then be written as

$$P_1 = 1 - \lambda^0 \exp(-\lambda)/0! = 1 - \exp(-\lambda), \quad (1)$$

where $\lambda = \rho S$ is the expected number of GRBs in the FRB error region S. The surface number density of GRBs is $\rho \approx 1440/41252.96 \approx 0.035/\text{deg}^2$. For a circular region with a radius δR (in unit of deg), we can derive its area $S \approx [41252.96(1 - \cos \delta R)]/2$.

To estimate the p-value of the chance coincidence, we adopt two approaches. First, for a conservative estimate, we use the uncertainty of $7'.5$ defined by the error bar of the FRB position, i.e., $\delta R = 0°.125$. We obtain the chance probability of having at least one (out of 1440) GRB whose distance to FRB 171209 is smaller than $0°.125$, which gives $P_1 \approx 0.0017$. The chance probability of having only one such association for all 110 FRBs can be estimated as $P = 1 - (1 - P_1)^{110} \approx 17.1\%$. We verify this simple estimate through Monte Carlo simulations. We randomly generate 1440 GRBs and 110 FRBs in the sky. Based on 10^5 simulations, the probability of having a GRB/FRB pair with a separation smaller than $0°.125$ is 17.4%, consistent with the analytical estimate.

One also needs to consider two other criteria for an association, i.e., the timing criterion (the GRB needs to occur before the FRB) and the redshift criterion (the maximum redshift derived from the FRB DM is larger than that of the GRB). To do this, we use the observed distributions of the detection time and redshift for both GRBs and FRBs to perform the simulations. As most GRBs were detected earlier than FRBs (FRBs were discovered much later than GRBs), adding the timing criterion does not reduce the chance probability significantly, i.e., ~14.1%. However, because the average redshift of GRBs is higher than the average maximum redshift of FRBs, adding the redshift criterion reduces the chance probability significantly to ~2.3%, which corresponds to a significance of 2.28σ.

Secondly, because GRB 110715A is well located inside the error circle of FRB 171209, one may use the angular distance between the centers of the error boxes of the two events, $0°.0836$, as δR.[11] One can obtain the chance probability of having at least one (out of 1440) GRB whose distance to FRB 171209 is smaller than $0°.0836$, i.e., $P_1 \approx 0.0007$. We also randomly generate 1440 GRBs and 110 FRBs in the sky. Based on 10^5 simulations, the chance probability of having one GRB/FRB pair with a separation smaller than $0°.0836$ is 7.6%. Considering the timing criterion, we obtain $P = 6.3\%$. When the redshift criterion is also considered, the final chance probability is 1.1%, which corresponds to a 2.55σ confidence level for the GRB 110715A/FRB 171209 association.

3. Is GRB 110715A Associated with FRB 171209?

Even though statistically one cannot establish a firm association between GRB 110715A and FRB 171209, it is nonetheless interesting to investigate whether physically such an association makes sense.

3.1. Magnetar as Central Engine of GRB 110715A

The Swift/BAT time-integrated spectrum of GRB 110715A can be well fitted with a Band function (Band et al. 1993), with $E_{\text{peak}} = 92.8 \pm 18.1$ keV, $\alpha = -1.23 \pm 0.12$, and $\beta = -2.05 \pm 0.19$ and $\chi^2 = 0.98$ (as shown in Figure 3). We obtained the isotropic γ-ray energy $E_{\gamma,\text{iso}} = (1.06 \pm 0.10) \times 10^{53}$ erg in the

---

[11] This approach was adopted by the IceCube team to claim a possible association between the neutrino trigger event IceCube-170922A and the blazar TXS 0506+056 (IceCube Collaboration et al. 2018).
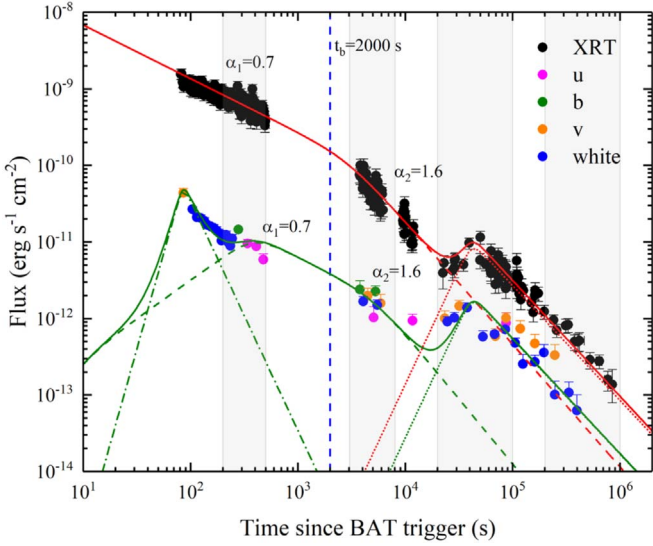
Figure 4. Light curves of X-ray and optical afterglows of GRB 110715A. The light curves are decomposed into multiple components (dashed or dashed–dotted lines). The solid lines represent the best fit to the data. The vertical blue dashed lines mark the break time between the shallow decay phase to the normal decay phase. The gray zones represent the time slices for the afterglow spectral energy distribution (SED) analysis.

Figure 5. SED analysis of GRB 110715A. Joint spectral fits of the X-ray and optical afterglows in four selected time intervals. The solid lines show the intrinsic power-law spectra derived from the joint fits. Different spectral bands are denoted in different symbols: XRT data (circle), white band (square), *b*-band (prismatic), *v*-band (triangle), and *u*-band (star). The photon indices Γ in different time intervals are also marked in different colors.

1–10^4 keV band. The results from the time-resolved spectral analysis show the "flux-tracking" pattern for E_p. To fit the GRB 110715A afterglow light curves, we employed a broken power-law function

$$F = F_1 \left[\left(\frac{t}{t_b} \right)^{\omega \alpha_1} + \left(\frac{t}{t_b} \right)^{\omega \alpha_2} \right]^{1/\omega}, \qquad (2)$$

where F_1 is the flux normalization, α_1 and α_2 are the afterglow flux decay indices before and after the break time (t_b), respectively, and ω is a smoothness parameter that represents the sharpness of the break. Figure 4 shows the X-ray and optical light curves of GRB 110715A. The X-ray light curve can be well fitted by a broken power-law function, with the best-fit power-law slope $\alpha_{X,1} = 0.70^{+0.04}_{-0.05}$ (shallow decay) before the break ($t_b = T_0 + 2.0^{+0.4}_{-0.3}$ ks) and $\alpha_{X,2} = 1.60^{+0.11}_{-0.09}$ (normal decay) after the break, respectively. There is a re-brightening component appearing at $\sim T_0 + 50^{+0.4}_{-0.3}$ ks. For the optical light curve, there is an early steep decay phase, which may be interpreted as the reverse shock emission as the ejecta is decelerated. This is followed by a shallow decay phase (with $\alpha_{O,1} = 0.70^{+0.13}_{-0.12}$) breaking at t_b and further decays with $\alpha_{O,2} = 1.60^{+0.15}_{-0.11}$. The re-brightening component also appeared in the optical afterglow. The result of the temporal analysis suggests that the X-ray and optical afterglow show an achromatic behavior (Wang et al. 2015).

We also analyze the spectral energy distributions (SEDs) of GRB 110715A afterglow, by jointly fitting the optical and XRT data with the Xspec package (Arnaud 1996) and the optical data that are corrected for Galactic extinction based on the burst direction, with $A_V = 0.030$, $A_R = 0.119$ and $A_I = 0.016$ (Schlafly & Finkbeiner 2011). The extinction in the host galaxy is also taken into account assuming an extinction curve similar to that of Small Magellanic Cloud (SMC) with its standard value of the ratio of total to selective extinction $R_{v,SMC} = 2.93$ (Pei 1992). The equivalent hydrogen column
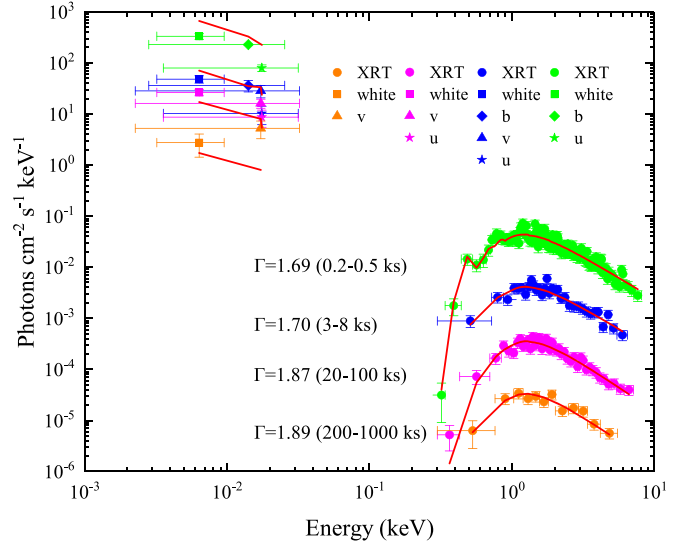
density of our Galaxy is $N_H = 4.33 \times 10^{21}$ cm^{-2}. The equivalent hydrogen column density of the host galaxy $N_H^{host} = (4.22 \pm 2.95) \times 10^{21}$ cm^{-2} is derived from the time-integrated XRT spectrum. We fix these values in our time-resolved spectral fits. We subdivided the broadband data into four temporal ranges (as marked in Figure 4). The SEDs of the joint optical and X-ray spectra can be well fitted with a single absorbed power-law function (as shown in Figure 5). The photon indices Γ (the spectral index $\beta = \Gamma - 1$) are 1.69, 1.70, 1.87, and 1.89 for the Slice 1 ($T_0 + [200, 500]$ s), Slice 2 ($T_0 + [3 \times 10^3, 8 \times 10^3]$ s), Slice 3 ($T_0 + [2 \times 10^4, 1 \times 10^5]$ s), and Slice 4 ($T_0 + [2 \times 10^5, 1 \times 10^6]$ s), respectively. There is no obvious spectral evolution observed in the afterglow phase. The temporal slopes of the normal decay phase ($\alpha_{X,II}$ and $\alpha_{O,II}$) are well consistent with the closure relations (α–β) of the fireball external shock model $\alpha = 3\beta/2 + 0.5 = 1.54 \pm 0.08$, which are located in spectral regime ($\nu_m < \nu < \nu_c$) in the wind stellar medium (e.g., Gao et al. 2013). For the shallow decay phase closure relation $\alpha = q/2 + (2 + q)\beta/2$ (Zhang et al. 2006), we obtained the energy injection parameter $q = 0$ for $\alpha_{X,I} = 0.70^{+0.04}_{-0.05}$ and $\alpha_{O,I} = 0.70^{+0.13}_{-0.12}$, which is consistent with the energy injection from the spindown of a millisecond magnetar (Dai & Lu 1998; Zhang & Mészáros 2001). Çıkıntoğlu et al. (2019) also argued that the millisecond magnetar could be the central engine of GRB 110715A.

We further investigate the afterglow data with the standard forward shock model with energy injection ($q = 0$). A Markov Chain Monte Carlo method is adopted to search for the best-fitting parameters. The results are shown in Figure 4. One can see that the model can well reproduce the data. The best-fitting parameters are: the isotropic kinetic energy $E_{K,iso} = 2 \times 10^{53}$ erg, the initial Lorentz factor $\Gamma_0 = 45$, the fraction of shock energy to electrons $\epsilon_e = 0.268$, the fraction of shock energy to magnetic fields $\epsilon_B = 1.1 \times 10^{-6}$, wind density parameter $A_* = 0.25$, the energy injection luminosity

$L_0 = 1 \times 10^{50}\,\mathrm{erg\,s^{-1}}$, and the duration of energy injection $t_b = 2000$ s. The fitting parameters are consistent with the statistical properties of a large sample of GRBs (e.g., Wang et al. 2015).

Because the energy injection $q = 0$ is well consistent with the magnetar spindown model, we can derive the magnetar parameters of GRB 110715A based on the data. The maximum energy is the total rotational energy of a millisecond magnetar and is defined as

$$E_{\mathrm{rot}} = \frac{1}{2}I\Omega_0^2 \simeq 2 \times 10^{52}\,\mathrm{erg}\,M_{1.4}R_6^2 P_{0,-3}^{-2}, \qquad (3)$$

where I is the moment of inertia, P_0 is the initial spin period, $\Omega_0 = 2\pi/P_0$ is the initial angular frequency of the neutron star, $M_{1.4} = M/1.4M_\odot$, and R is the radius of the magnetar. The isotropic γ-ray and kinetic energies are larger than this value, suggesting that the outflow is beamed, with a beaming factor $f_b = 1 - \cos\theta_j < 0.1$, where θ_j is the half opening angle of the jet. Based on the characteristic spindown luminosity L_0 and the spindown timescale τ of a magnetar as shown in Equations (6) and (8) in Zhang & Mészáros (2001), one can calculate the surface polar cap magnetic field strength B_p and the initial spin period P_0:

$$B_{\mathrm{p},15} = 2.05(I_{45}R_6^{-3}L_{0,49}^{-1/2}\tau_3^{-1})\,\mathrm{G}, \qquad (4)$$

$$P_{0,-3} = 1.42(I_{45}^{1/2}L_{0,49}^{-1/2}\tau_3^{-1/2})\,\mathrm{s}. \qquad (5)$$

Observationally, the spindown luminosity L_0 can be generally written as (Lü & Zhang 2014)

$$L_0 = [L_{\mathrm{X,iso}} + E_{\mathrm{K,iso}}(1 + z)/t_b]f_b, \qquad (6)$$

where $L_{\mathrm{X,iso}}$ is the X-ray luminosity due to internal dissipation of the magnetar wind, which is negligible in our case.

As no jet break is observed in GRB 110715A, we can use the epoch of the last observational data point to set a lower limit on θ_j (Wang et al. 2018b), i.e., $\theta_j > 6°.2$. Using $E_{\mathrm{K,iso}} = 2 \times 10^{53}$ erg, $L_{\mathrm{X,iso}} = 3.28 \times 10^{47}\,\mathrm{erg\,s^{-1}}$, and $\tau = t_b/(1 + z) = 2000/(1 + 0.82) = 1099$ s, we obtain $P_0 < 3.59$ ms and $B_p < 4.95 \times 10^{15}$ G, respectively. These parameters fall into the regime of typical young magnetars for GRB central engines. Such a magnetar is believed to power repeating FRBs when the environment becomes clean (Murase et al. 2016; Metzger et al. 2017; Margalit & Metzger 2018).

3.2. Is the Magnetar the Progenitor of FRB 171209?

As reported by Osłowski et al. (2019), FRB 171209 has a duration of $\Delta t \sim 0.138$ ms and a fluence of $f_\nu \gtrsim 3.7$ Jy ms at $\nu \sim 1$ GHz. If FRB 171209 is indeed associated with GRB 110715A, according to the redshift $z = 0.82$ of GRB 110715A, the luminosity distance is $d_{\mathrm{L}} \simeq 5$ Gpc. The isotropic energy of FRB 171209 is about $E_{\mathrm{FRB}} \sim 4\pi d_{\mathrm{L}}^2\nu f_\nu \gtrsim 1.1 \times 10^{41}$ erg. If this energy is provided by the magnetic energy of the underlying magnetar, one may place a most demanding constraint on the strength of the magnetic field of the underlying magnetar assuming isotropic FRB radiation. The emission radius can be approximately estimated as $r_e \sim c\Delta t \simeq 4.1 \times 10^6$ cm. The magnetic field strength at r_e should satisfy

$$\frac{B^2}{8\pi}\left(\frac{4\pi}{3}r_e^3\right) \gtrsim E_{\mathrm{FRB}}, \qquad (7)$$

where $B = B_{\mathrm{p}}(r_e/R)^{-3}$. Therefore, the observation of FRB 171209 demands that the surface polar cap magnetic field strength is

$$B_{\mathrm{p}} \gtrsim \left(\frac{6Er_e^3}{R^6}\right)^{1/2} \simeq 6.8 \times 10^{12}\,\mathrm{G}, \qquad (8)$$

which is consistent with the observation constraints derived from the afterglow emission of GRB 110715A.

According to the redshift $z = 0.82$ of GRB 110715A, the DM contribution from the IGM is given by (Zhang 2018a),

$$\mathrm{DM}_{\mathrm{IGM}} \simeq 855\,\mathrm{pc\,cm^{-3}}z \simeq 700\,\mathrm{pc\,cm^{-3}}, \qquad (9)$$

and the local DM from the host galaxy is

$$\mathrm{DM}_{\mathrm{host}} = (1 + z)(\mathrm{DM}_{\mathrm{E}} - \mathrm{DM}_{\mathrm{IGM}}) \simeq 950\,\mathrm{pc\,cm^{-3}} \qquad (10)$$

where $\mathrm{DM}_{\mathrm{E}} = \mathrm{DM} - \mathrm{DM}_{\mathrm{gal}} = 1222.4\,\mathrm{pc\,cm^{-3}}$ is the extragalactic DM of FRB 171209 (Osłowski et al. 2019).

At $z = 0.82$, the uncertainty of the IGM DM is $\sigma_{\mathrm{IGM}} \sim 200\,\mathrm{pc\,cm^{-3}}$ (McQuinn 2014). Meanwhile, because the host galaxy of GRB 110715A is similar to that of FRB 121102, we take the DM contribution from the interstellar medium (ISM) as $\mathrm{DM}_{\mathrm{ISM}} \lesssim 200\,\mathrm{pc\,cm^{-3}}$ (Sánchez-Ramírez et al. 2017; Tendulkar et al. 2017). Therefore, even considering the large-scale structure fluctuation and a possible large DM from the ISM, there is still a large DM excess $\mathrm{DM}_{\mathrm{loc}} \sim 550\,\mathrm{pc\,cm^{-3}}$. This DM excess is likely contributed by the GRB-associated SN occurred $t \simeq 6.4$ yr before FRB 171209. In the free-expansion phase, the DM provided by a young supernova remnant (SNR) with mass M and kinetic energy E_{SN} can be estimated as (e.g., Piro 2016; Yang & Zhang 2017)

$$\mathrm{DM}_{\mathrm{SN}} = \frac{\eta M^2}{8\pi\mu_m m_p E_{\mathrm{SN}} t^2} = 630\,\mathrm{pc\,cm^{-3}}$$
$$\times\, \eta\left(\frac{M}{M_\odot}\right)^2\left(\frac{t}{6.4\,\mathrm{yr}}\right)^{-2}\left(\frac{E_{\mathrm{SN}}}{10^{51}\,\mathrm{erg}}\right)^{-1} \qquad (11)$$

where $\mu_m = 1.2$ is the mean molecular weight for a solar composition in the SNR ejecta, and η is the ionization fraction of the medium in the SNR. We can see that for a typical SN with a few times solar masses, the corresponding DM contribution could reach the required host-galaxy DM of FRB 171209. One should check the the free–free absorption in the SN. For a young SNR, the free–free optical depth through the ejecta shell is

$$\tau_{\mathrm{ff}} \simeq (0.018T^{-3/2}Z^2 n_e n_i \nu^{-2}\bar{g}_{\mathrm{ff}})\mathcal{L} \simeq 3600\left(\frac{T}{10^4\,\mathrm{K}}\right)^{-3/2}$$
$$\times\left(\frac{M}{M_\odot}\right)^{9/2}\left(\frac{E_{\mathrm{SN}}}{10^{51}\,\mathrm{erg}}\right)^{-5/2}\left(\frac{t}{1\,\mathrm{yr}}\right)^{-5}\left(\frac{\nu}{1\,\mathrm{GHz}}\right)^{-2}, \qquad (12)$$

where n_e and n_i are the number densities of electrons and ions, respectively, and $n_e = n_i$ and $Z = 1$ are assumed for an ejecta with a fully ionized hydrogen-dominated composition, $\mathcal{L} \sim r \sim vt$ is the ejecta thickness, and $\bar{g}_{\mathrm{ff}} \sim 1$ is the Gaunt factor. If the SNR ejecta is transparent for FRB, i.e., $\tau_{\mathrm{ff}} \lesssim 1$,

one gets the SNR age (e.g., Yang et al. 2019b)

$$t \gtrsim 5\,\mathrm{yr} \left(\frac{M}{M_\odot} \right)^{9/10} \left(\frac{E_{\mathrm{SN}}}{10^{51}\,\mathrm{erg}} \right)^{-1/2}, \qquad (13)$$

where $\nu \sim 1$ GHz and $T \sim 10^4$ K are taken. This is consistent with the 6.4 yr time delay between FRB 171209 and GRB 110715A.

4. Summary and Discussions

Lacking multiwavelength observational data of FRBs, it is hard to constrain their physical origin. It has been suggested that at least some FRBs may be physically associated with GRBs (Zhang 2014; Metzger et al. 2017). The GRB may leave behind a long-lived magnetar, which may produce FRBs through ejecting magnetosphere upon collapse Falcke & Rezzolla (2014), or more likely, produce repeated bursts through crust cracking or magnetic reconnection (e.g., Popov & Postnov 2010; Katz 2016; Beloborodov 2017; Kumar et al. 2017; Yang & Zhang 2018; Wang et al. 2018a).

We searched for possible GRB–FRB associations based on the localization data of 110 FRBs and the precise localization data of 1440 GRB afterglows. We found that the long-duration GRB 110715A is within the error box of FRB 171209 and the redshift of the GRB 110715A is lower than the maximum redshift derived from the DM of the FRB 171209. Taking the factors of spatial location, time of occurrence, and the redshift criterion, we derive a chance probability of 2.3%–1.1%, corresponding to a 2.28σ–2.55σ confidence level for the association.

Even though the chance coincidence probability cannot establish a firm association between GRB 110715A and FRB 171209, we nonetheless investigated whether there exists a self-consistent physical picture to make a connection between the two. We modeled the afterglow of GRB 110715A and identified a shallow decay signature, which is consistent with energy injection by a millisecond magnetar with $P_0 < 3.59$ ms and $B_{\mathrm{p}} < 4.59 \times 10^{15}$ G. With the Milky Way and IGM contributions subtracted, the observed DM of FRB 171209 has an excess of ~ 950 pc cm^{-3}, which is consistent with the DM contribution of a young (~ 6.4 yr old) SNR associated with GRB 110715A with a few solar masses and kinetic energy $E_{\mathrm{SN}} \sim 10^{51}$ erg. The requirement that the free–free optical depth $\tau_{\mathrm{ff}} \lesssim 1$ suggests that FRBs can be observable only a few years after the explosion, consistent with the observed 6.4 yr delay between GRB 110715A and FRB 171209. FRB 171209 so far does not show a repeating behavior. Its light curve shows one single pulse without a noticeable temporal structure (Osłowski et al. 2019). The intrinsic duration is sub-millisecond. In principle, the burst could be an one-off event. If it is associated with GRB 110715A, it may be related to the collapse of the supramassive neutron star at such a late epoch (Falcke & Rezzolla 2014; Zhang 2014). However, contrived conditions are needed to allow the collapsing time to be at such a late stage after the spindown timescale. More likely, FRB 171209 may be one of many repeating bursts powered by the magnetar harbored in GRB 110715A (Murase et al. 2016; Metzger et al. 2017). Searching for repeating bursts from FRB 171209 would be essential to test this possibility.

Observationally, no SN was reported for GRB 110715A (Sánchez-Ramírez et al. 2017). This is not surprising, as GRB 110715A is not nearby and is a high-luminosity long GRB with a bright optical afterglow. The SN signature is likely outshone by the afterglow. It is well known that essentially every long GRB is accompanied by a SN Ic (Woosley & Bloom 2006), so that invoking a SN to account for the extra DM from FRB 171209 is justified.

ORCID iDs

Xiang-Gao Wang https://orcid.org/0000-0001-8411-8011
Yuan-Pei Yang https://orcid.org/0000-0001-6374-8313
Bing Zhang https://orcid.org/0000-0002-9725-2524
Da-Bin Lin https://orcid.org/0000-0003-1474-293X
En-Wei Liang https://orcid.org/0000-0002-7044-733X

References

Arnaud, K. A. 1996, in ASP Conf. Ser. 101, Astronomical Data Analysis Software and Systems V, ed. G. H. Jacoby & J. Barnes (San Francisco, CA: ASP), 17
Band, D., Matteson, J., Ford, L., et al. 1993, ApJ, 413, 281
Bannister, K. W., Deller, A. T., Phillips, C., et al. 2019, Sci, 365, 565
Bannister, K. W., Murphy, T., Gaensler, B. M., & Reynolds, J. E. 2012, ApJ, 757, 38
Beloborodov, A. M. 2017, ApJL, 843, L26
Briggs, M. S., Paciesas, W. S., Pendleton, G. N., et al. 1996, ApJ, 459, 40
Callister, T., Kanner, J., & Weinstein, A. 2016, ApJL, 825, L12
Casentini, C., Verrecchia, F., Tavani, M., et al. 2020, ApJL, 890, L32
Chatterjee, S., Law, C. J., Wharton, R. S., et al. 2017, Natur, 541, 58
CHIME/FRB Collaboration, Andersen, B. C., Bandura, K., et al. 2019, ApJL, 885, L24
Çıkıntoğlu, S., Sasmaz Mus, S., & Eksi, K. Y. 2019, arXiv:1910.00554
Cordes, J. M., & Chatterjee, S. 2019, ARA&A, 57, 417
Cunningham, V., Cenko, S. B., Burns, E., et al. 2019, ApJ, 879, 40
Dai, Z. G., & Lu, T. 1998, A&A, 333, L87
Dai, Z. G., Wang, J. S., Wu, X. F., & Huang, Y. F. 2016, ApJ, 829, 27
de Ugarte Postigo, A., Lundgren, A., Mac-Auliffe, F., et al. 2011, GCN, 12168, 1
DeLaunay, J. J., Fox, D. B., Murase, K., et al. 2016, ApJL, 832, L1
Eftekhari, T., Berger, E., Margalit, B., et al. 2019, ApJL, 876, L10
Evans, P. A., & Sonbas, E. 2011, GCN, 12165, 1
Falcke, H., & Rezzolla, L. 2014, A&A, 562, A137
Gao, H., Lei, W.-H., Zou, Y.-C., Wu, X.-F., & Zhang, B. 2013, NewAR, 57, 141
Gao, H., & Zhang, B. 2017, ApJ, 835, L21
Golenetskii, S., Aptekar, R., Frederiks, D., et al. 2011, GCN, 12166, 1
Guidorzi, C., Marongiu, M., Martone, R., et al. 2019, ApJ, 882, 100
Hancock, P. J., Murphy, T., & Schmidt, B. P. 2011, GCN, 12171, 1
IceCube Collaboration, Aartsen, M. G., Ackermann, M., et al. 2018, Sci, 361, eaat1378
Ioka, K., & Zhang, B. 2020, ApJL, 893, L26
Kashiyama, K., Ioka, K., & Mészáros, P. 2013, ApJL, 776, L39
Katz, J. I. 2016, ApJ, 826, 226
Kuin, N. P. M., & Sonbas, E. 2011, GCN, 12162, 1
Kumar, P., Lu, W., & Bhattacharya, M. 2017, MNRAS, 468, 2726
Lorimer, D. R., Bailes, M., McLaughlin, M. A., Narkevic, D. J., & Crawford, F. 2007, Sci, 318, 777
Liu, T., Romero, G. E., Liu, M.-L., & Li, A. 2016, ApJ, 826, 82
Lü, H.-J., & Zhang, B. 2014, ApJ, 785, 74

MAGIC Collaboration, Acciari, V. A., Ansoldi, S., et al. 2018, MNRAS, 481, 2479
Marcote, B., Nimmo, K., Hessels, J. W. T., et al. 2020, Natur, 577, 190
Margalit, B., Berger, E., & Metzger, B. D. 2019, ApJ, 886, 110
Margalit, B., & Metzger, B. D. 2018, ApJL, 868, L4
McQuinn, M. 2014, ApJL, 780, L33
Men, Y., Aggarwal, K., Li, Y., et al. 2019, MNRAS, 489, 3643
Mészáros, P. 2006, RPPh, 69, 2259
Metzger, B. D., Berger, E., & Margalit, B. 2017, ApJ, 841, 14
Murase, K., Kashiyama, K., & Mészáros, P. 2016, MNRAS, 461, 1498
Nelson, P. 2011, GCN, 12174, 1
Osłowski, S., Shannon, R. M., Ravi, V., et al. 2019, MNRAS, 488, 868
Palaniswamy, D., Wayth, R. B., Trott, C. M., et al. 2014, ApJ, 790, 63
Pei, Y. C. 1992, ApJ, 395, 130
Petroff, E., Bailes, M., Barr, E. D., et al. 2015, MNRAS, 447, 246
Petroff, E., Barr, E. D., Jameson, A., et al. 2016, PASA, 33, e045
Petroff, E., Hessels, J. W. T., & Lorimer, D. R. 2019, A&ARv, 27, 4
Piranomonte, S., Vergani, S. D., Malesani, D., et al. 2011, GCN, 12164, 1
Piro, A. L. 2016, ApJL, 824, L32
Platts, E., Weltman, A., Walters, A., et al. 2019, PhR, 821, 1
Popov, S. B., & Postnov, K. A. 2010, in Proc. Conf. Dedicated to Viktor Ambartsumian's 100th Anniversary, Evolution of Cosmic Objects Through Their Physical Activity, ed. H. A. Harutyunian, A. M. Mickaelian, & Y. Terzian (Yerevan: NAS RA), 129
Prochaska, J. X., Macquart, J.-P., McQuinn, M., et al. 2019, Sci, 366, 231
Ravi, V., Catha, M., D'Addario, L., et al. 2019, Natur, 572, 352
Sánchez-Ramírez, R., Hancock, P. J., Jóhannesson, G., et al. 2017, MNRAS, 464, 4624
Schlafly, E. F., & Finkbeiner, D. P. 2011, ApJ, 737, 103
Scholz, P., Spitler, L. G., Hessels, J. W. T., et al. 2016, ApJ, 833, 177
Sonbas, E., Barthelmy, S. D., Baumgartner, W. H., et al. 2011, GCN, 12158, 1
Tavani, M., Verrecchia, F., Casentini, C., et al. 2020, ATel, 13446, 1

Tendulkar, S. P., Bassa, C. G., Cordes, J. M., et al. 2017, ApJL, 834, L7
Thornton, D., Stappers, B., Bailes, M., et al. 2013, Sci, 341, 53
Tingay, S. J., & Yang, Y.-P. 2019, ApJ, 881, 30
Totani, T. 2013, PASJ, 65, L12
Ukwatta, T. N., Barthelmy, S. D., Baumgartner, W. H., et al. 2011, GCN, 12160, 1
Updike, A. C., Schady, P., Greiner, J., et al. 2011, GCN, 12169, 1
Wang, F. Y., Wang, Y. Y., Yang, Y.-P., et al. 2020, ApJ, 891, 72
Wang, J.-S., Yang, Y.-P., Wu, X.-F., Dai, Z.-G., & Wang, F.-Y. 2016, ApJL, 822, L7
Wang, W., Luo, R., Yue, H., et al. 2018a, ApJ, 852, 140
Wang, X.-G., Zhang, B., Liang, E.-W., et al. 2015, ApJS, 219, 9
Wang, X.-G., Zhang, B., Liang, E.-W., et al. 2018b, ApJ, 859, 160
Woosley, S. E., & Bloom, J. S. 2006, ARA&A, 44, 507
Xi, S.-Q., Tam, P.-H. T., Peng, F.-K., & Wang, X.-Y. 2017, ApJL, 842, L8
Yamasaki, S., Totani, T., & Kawanaka, N. 2016, MNRAS, 460, 2875
Yang, Y.-H., Zhang, B.-B., & Zhang, B. 2019a, ApJL, 875, L19
Yang, Y.-P., & Zhang, B. 2017, ApJ, 847, 22
Yang, Y.-P., & Zhang, B. 2018, ApJ, 868, 31
Yang, Y.-P., Zhang, B., & Wei, J.-Y. 2019b, ApJ, 878, 89
Yi, S.-X., Gao, H., & Zhang, B. 2014, ApJL, 792, L21
Zhang, B. 2014, ApJL, 780, L21
Zhang, B. 2016, ApJL, 827, L31
Zhang, B. 2017, ApJL, 836, L32
Zhang, B. 2018a, ApJL, 867, L21
Zhang, B. 2018b, The Physics of Gamma-Ray Bursts (Cambridge: Cambridge Univ. Press)
Zhang, B. 2020, ApJL, 890, L24
Zhang, B., Fan, Y. Z., Dyks, J., et al. 2006, ApJ, 642, 354
Zhang, B., & Mészáros, P. 2001, ApJL, 552, L35
Zhang, B.-B., & Zhang, B. 2017, ApJL, 843, L13